Università degli Studi di Padova
Dipartimento di Fisica ed Astronomia "Galileo Galilei"

Corso di laurea triennale in Fisica

Characterization of Silicon Photomultipliers for Cherenkov Telescope Applications

Relatore: **Riccardo Rando** Laureanda: **Lea Pennacchioni**

Anno accademico 2014/2015
Sessione di Laurea Estiva

Contents

Chapter 1

Introduction

1.1 Thesis objective and structure

The primary objective of this thesis is the characterization of a novel silicon photomultiplier prototype developed by FBK (*Fondazione Bruno Kessler*) for near-ultraviolet (near-UV) light detection, called NUV-SiPM . The sensor used is the SiPM-NUV 18.

This thesis is divided into five chapters: chapter 1 introduces the reader to gamma-ray astronomy and presents the IACT (*Imaging Atmospheric Cherekov Technique*) and the CTA (*Cherenkov Telescopes Array*) project. Chapter 2 introduces the different types of photodetectors used in the low photon flux detection, and in particular describes the various figures of merit to characterize SiPMs.
In chapter 3, the experimental measurements and the analysis techniques are presented and discussed. Finally in chapter 4, the obtained results are analyzed, compared and discussed.
The appendixes describe the instrumentation used during the experiments and a measure of the speed of light.

1.2 Gamma-ray astronomy

Gamma-ray astronomy consists in the observation of gamma radiation emitted by extraterrestrial bodies. This radiation is located at the top of the radiation spectrum, with wavelengths in the order of 10^{-12} m and energies of 10^6 eV and higher. Gamma radiation can give important information regarding cosmic accelerators. In particular this radiation is not deviated by magnetic fields, therefore it allows to image what happens in the emission regions.

Gamma rays can be generated in several ways:

- **High energy gamma rays** are produced when highly relativistic particles, accelerated for example in the gigantic shock waves of stellar explosions, collide with ambient gas, or interact with photons and magnetic fields. They can also be produced by decays of heavy particles such as hypothetical dark matter particles.

- **Low energy gamma rays** can be produced by the curvature of charged particles in radiation fields or by processes of decay (e.g. π_0) and annihilation (e.g. electron-positron) and lastly by nuclear lines.

Direct detection of gamma rays is only possible by means of satellites since the atmospheric opacity increases rapidly at high energies (see Fig. 1.1). However ground based Cherenkov telescopes, allow the detection of Cherenkov radiation by making the atmosphere itself part of the detector.

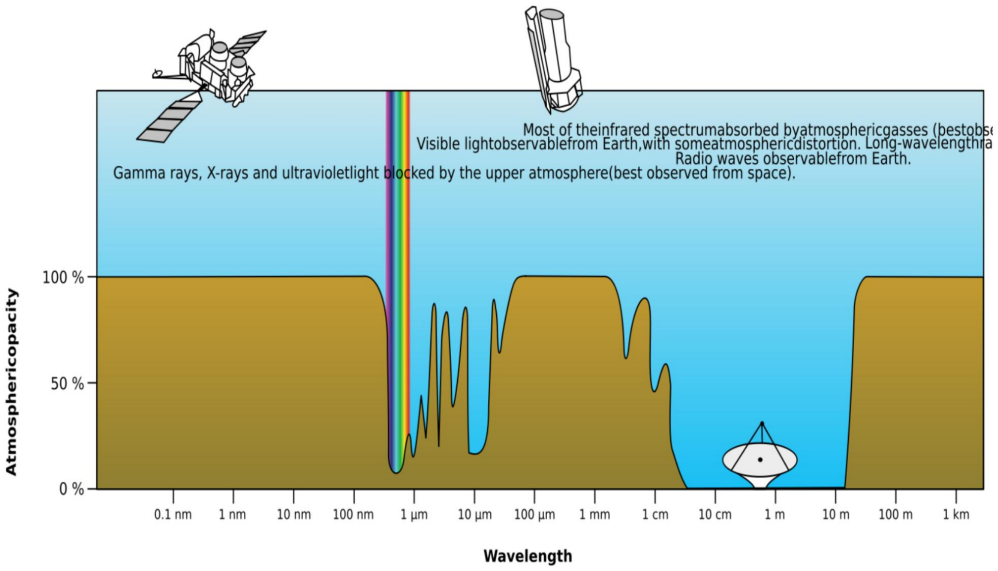

Figure 1.1: Plot of Earth's atmospheric opacity to electromagnetic radiation of various wavelengths. (Image courtesy of Wikipedia.)

The ground based telescopes detect gamma radiation indirectly, by means of the Cherenkov light produced by air showers: when a very high energy gamma ray enters the atmosphere, it interacts with atmospheric nuclei and generates a shower of secondary electrons, positrons and photons. These charged particles move in the atmosphere at speeds beyond the speed of

light in the gas and produce a radiation. This is called Cherenkov radiation and it is characterized by a typical spectrum peaked in the UV region.

This light is captured and reflected by the ground based telescopes' camera mirrors and is used to image the shower. Reconstructing the shower axis in space and tracing back the source's location in the sky allows the celestial origin of the gamma ray to be determined. This is known as IACT (Imaging Atmospheric Cherenkov Telescopes). This technique allows the detection of VHE (Very High Energy, E>10GeV) gamma rays, which would require prohibitively large effective detection area in the space telescopes. Several experiments have been known for their groundbreaking discoveries, but being the known sources too few, real statistical studies of population are impossible at this stage. A solution to this problem would be to collect more statistics, but the construction of bigger telescopes is expensive and very complicated. The general idea is to create an array of several telescopes in order to cover a bigger area. By using different types of telescopes they can be optimized to the shower properties at different energies, thus covering with high efficiency a broad energy range.

The CTA (Cherenkov Telescope Array) is a ground-based gamma-ray observatory currently under development by an international consortium with more than 1000 members from 27 countries. Current plans call for the observatory to comprise two separate arrays – one in the Northern Hemisphere and one in the Southern Hemisphere – totaling more than 100 telescopes of three different sizes.

In a possible design scenario, the southern hemisphere array of CTA will consist of three types of telescopes with different mirror sizes in order to cover the full energy range. The northern hemisphere array would consist of the two larger telescope types. The different types of telescopes will be used in order to sample different energy intervals:

- The low energy instrumentation will consist of a few 24 meter-class telescopes with a moderate field of view (FoV) of the order of 4-5 degrees.
- The medium energy range, from around 100 GeV to 1 TeV, will be covered by telescopes of the 10-12 meter class with a FoV of 6-8 degrees.
- The high energy instruments, operating above 10 TeV, will consist of a large number of small (4-6 meter diameter) telescopes with a FoV of around 10 degrees.

This thesis covers Silicon photo multipliers, which are photo detectors thought to be adequate to be used in Cherenkov telescopes. Being the radiation flux low, the telescopes camera must be capable to detect single photons.

In particular they have to be fast enough to detect showers of the duration of a few ns and with a PDE good enough to detect one or a few photons.

Chapter 2

Single photon detectors

2.1 Introduction to Photo detectors

A photo detector is a sensor that converts light energy into an electrical signal. One of the first photo detectors were the Photomultiplier Tubes (PMT's) which dominated the field of low photon flux detection for more than 50 years, practically without alternative. The PMT is a vacuum tube structure consisting of an input window, a photo-cathode with a low work function and an electron multiplier sealed into an evacuated glass tube. Photons release electrons from the photocatode, which are accelerated by the high electrical field between the metal elements inside the tube (dynodes), to the point that they can produce secondary electrons each time they collide with one, causing a multiplication of the signal. The electron multiplication process gives the PMT an internal gain of 10^6 - 10^7 , which makes them suitable for single photon counting. PMTs can be designed to peak this efficiency in the blue region of the spectrum, to match the characteristics of the Cherenkov light.

Despite the overwhelming success, these detectors have some issues, such as high price, bulky shape and sensibility to magnetic fields. Concerning modern semiconductor structures for photon detection, Avalanche Photo Detectors (APD) have been developed as a serious alternative to PMTs. The basic principle of a semiconductor-based photon detector is to create a structure with a region free from charge carriers, called depletion area, and a method to transport the charge. This can be achieved by means of *pn*-junction. Photons with energy higher than the band-gap of the semiconductor are absorbed in the depleted area and create an electron-hole pair. Carriers, generated by the photon, are separated by a build-in electric field: electrons drift to the positive enhanced region (*n*-region), holes to the negative enhanced region (*p*-region); this current can be amplified and read out with proper instrumen-

tation. APDs are smaller than the PMTs, also avalanche photo-diodes that are operated with a high voltage bias have an intense electric field, which leads to avalanche multiplication of the electron signal, effectively achieving something close to the PMT amplification mechanism with an output current proportional to the input of the photon flux. However, to achieve the best signal to noise response, the APDs are operated with a lower gain than the PMT. The main problem of APDs is that gain is limited by the excess noise given by the fluctuations of avalanche multiplication.

Limitations in gain and most of the stability problems can be avoided in small area APDs by operating them in the limited Geiger mode instead of in the proportional gain mode, i.e. by increasing the bias voltage slightly (10%-20%) above breakdown voltage. This way, a single electron can trigger a diverging avalanche multiplication process which, differently from the proportional mode avalanche where basically only electrons generate additional electron hole pairs, is diverging because both electrons and holes actively participate in the multiplication process. The avalanche created in GAPD (Geiger mode Avalanche Photo Diode) creates a self sustained constant current. By means of a quenching system the breakdown can be controlled and rapidly terminated (the process lasts $\sim$ 1 ns), thus readying the sensor for another detection. This process is called passive quenching. The passive quenching isn't the only quenching scheme, other more complex schemes are possible but they will not be illustrated in this thesis. A simple way to achieve the passive quenching is by inserting a high Ohmic resistor in series to the diode. After quenching, the resistor prevents an instantaneous recharge of the diode capacitance and an instantaneous reset to the initial bias above breakdown. Due to the diverging nature of the multiplication, any information about the primary signal (i.e. the number of generated photoelectrons) that initiated the breakdown is lost.
APDs operated in the Geiger mode have the advantage of large, well defined output pulses ($10^5 \sim 10^7$ electrons) per breakdown, and can be used for "single photon counting". Therefore, such APDs are often referred to as Single Photon Avalanche Diodes (SPADs).

2.2 SiPM

A SiPM (Silicon Photo Multiplier) is an array of typically 100 up to 10,000 SPADs per mm^2. It is a photo detector that makes use of the advantages of GAPD and, at the same time, allows to retain over a large dynamic range the information on the number of primary photoelectrons. In this device, each SPAD has its own miniature, integrated quenching resistor. In addition, all SPAD-resistor combinations (called *cells* thereafter) are connected in parallel to a common bus. (Figure 2.1).

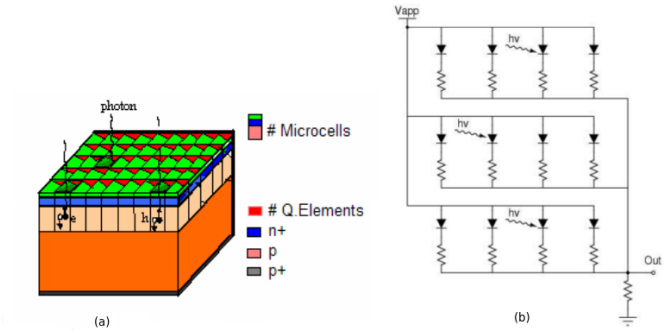

Figure 2.1: (a) Equivalent schematic of the structure of the SiPM. (b) Simplified circuit of a SIPM [1].

The output signal of the device is the analog sum signal of all "fired" cells. Figure 2.2 shows in the left panel the top view of four cells of such a device: each photosensitive area is surrounded by an insensitive region, separating cells from each other.

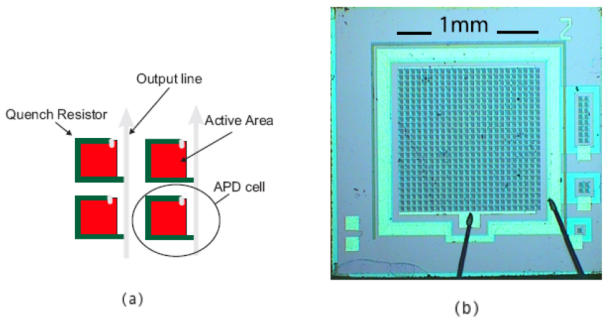

Figure 2.2: (a) Sketch of 4 cells of a SiPM. Each cell consists of a photo diode and a quenching resistor (green) that is connected in series between the diode and the readout line [5]. (b) Picture of a SiPM (taken from the Internet).

The most critical figures of merit which should be optimized in a GAPD in order to make it suitable for the application are decribed below:

2.2.1 Photon Detection Efficiency

The photon detection efficiency (PDE) is the statistical probability of detecting a photon impinging on the SiPM surface. The PDE is the product of the following factors: quantum efficiency QE, triggering probability P_i, geometric fill factor ϵ.

$$PDE = QE \cdot P_i \cdot \epsilon \tag{2.1}$$

Quantum efficiency is defined as the average number of electron–hole pairs created by conversion of one photon in the depleted layer of a semiconductor.

Triggering Probability is the probability for a single electron of triggering a breakdown.

Geometric fill factor is defined as the ratio of the photo sensitive area A_S to the total area A_{TOT} of the device: $\epsilon = \frac{A_S}{A_{TOT}}$.

2.2.2 Gain

One of the most important features of the SiPM is its intrinsic and stable high gain. The gain of the SiPM is given by:

$$G = \frac{Q_{tot}}{n_{ph} \cdot q} \tag{2.2}$$

where Q_{tot} is the output charge produced by n_{ph} detected photons, and q is the charge of an electron. Assuming that on average a photon produces the avalanche of one pixel the gain is given by:

$$G = \frac{Q_{pixel}}{q} = \int \frac{I}{q} dt \sim C_D \frac{V - V_b}{q} \sim A \tag{2.3}$$

Where C_D is the diode capacitance and A is the amplitude of the current pulse produced when any of the cells goes to breakdown. When many cells are fired at the same time the output is the sum of individual pulses.

2.2.3 Dark Rate

An avalanche breakdown in a SiPM can be triggered by a photo-generated carrier, when photons strike the detector, or by thermally-generated free carriers in, or close to, the depleted region. The pulses generated by these two processes are indistinguishable from each other. The latter represents the intrinsic noise of the silicon photomultiplier and the frequency of such noise can be determined by counting the pulses occurring per second when the SiPM is in dark condition. The signal produced by these so called "dark counts" is affected by both afterpulsing and crosstalk (see later), so one can more accurately estimate the "primary dark rate" by factoring out the contribution of these two unrelated effects.

Primary Dark Events : A breakdown can be triggered by an incoming photon or by any generation of free carriers. The latter produces dark counts with a rate of 100 KHz to several MHz per mm^2 at 25^o C. Carriers in the conduction band may be generated by the electric field or by thermal agitation. Thermally generated carriers can be reduced by cooling the device. Another possibility is to operate the GAPD at a lower bias voltage resulting in a smaller electric field and thereby lower gain.

Crosstalk : The crosstalk effect is due to the fact that a pulse current produced by a pixel, caused by a photon detection event or a primary noise event, can induce one or more adjacent pixels to experience the avalanche breakdown. The corresponding output pulse current has then the amplitude peak proportional to the number of involved pixels in the single photo-detection and in the correlated crosstalk phenomena. The crosstalk noise has two different physical origins: optical and electrical. The noise contribution is mainly due to the optical crosstalk, which is related to the fact that in an avalanche breakdown there are in average 3 photons emitted per 10^5 carriers with a photon energy higher than 1.14 eV, the band gap of silicon. When these photons travel to a neighboring cell, they can trigger a breakdown there, as any external photon (see Fig. 2.3).

Crosstalk effect causes an excess signal during light measurements, therefore when n photons arrive on the SiPM a signal proportional to n+1 can be measured with a probability PCT called crosstalk probability. In order to reduce the crosstalk between neighboring pixels two main strategies have been studied: the first consists in incrementing the distance between cells, while second one consists in fabricating trenches, filled with optical absorbing material, all around each cell (see Fig. 2.4).

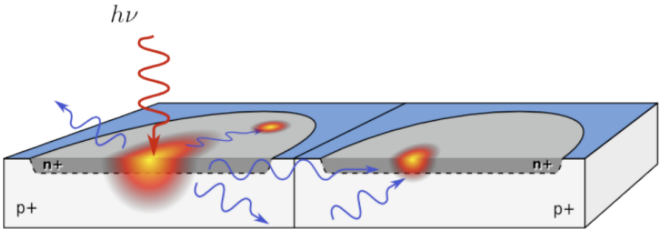

Figure 2.3: Optical crosstalk between neighboring cells [7].

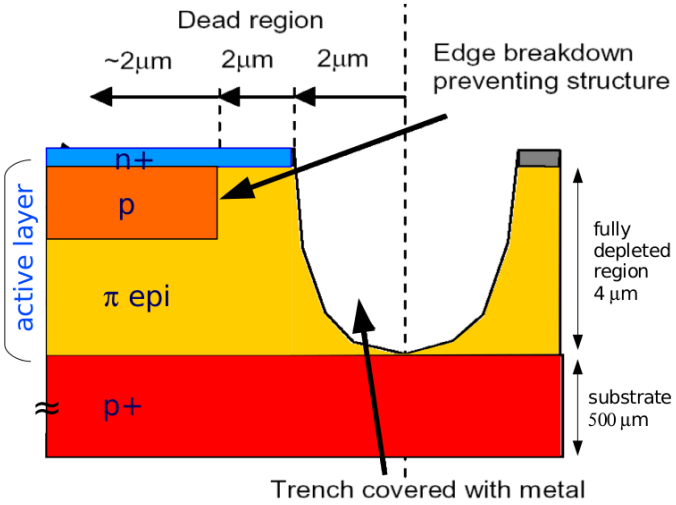

Figure 2.4: Close up of the SiPM cell [4].

This design allows to reduce considerably the crosstalk while affecting mildly the geometrical fill factor and therefore the overall efficiency.

Afterpulsing : Carriers can be trapped and released after a certain time Δt, causing a delayed avalanche in the same pixel where the breakdown occurred, called afterpulse. These second pulses have a pulse height that is smaller that usual, since the cell was not completely charged. Afterpulses cause noise in the distribution of pulse peak height.

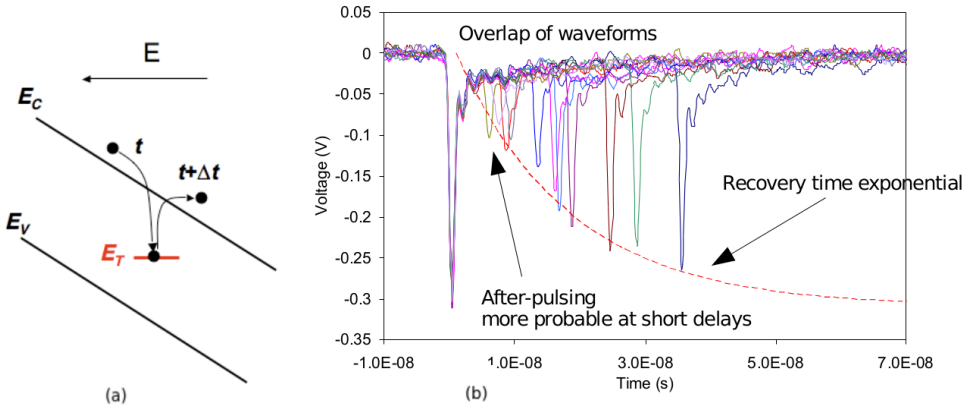

Figure 2.5: (a) Trapping and delayed releasing of a free carrier produced during an avalanche breakdown by impurity in the depleted volume of the function. (b)Primary pulse and afterpulse. [9]

2.2.4 Timing

The timing of the SiPM is the statistical distribution of the delays from the true arrival time of the photons and the actual detection time registered by the electrical output of the detector. A typical timing resolution of a SiPM ($\sim<$ 1 ns) presents a main peak due to the photon absorbed in the depletion region and a slow tail due to photons absorbed in the neutral regions beneath the junction which reach the electric field region by diffusion.

2.2.5 Dynamic range

A SiPM can not detect more photons than the number of available cells. Formally, the detection of photons by a silicon photomultiplier is a statistical process based on the probability of detecting randomly distributed photons by a limited number of sensitive micro cells. The output signal of the device is not directly proportional to the number of photoelectrons but it is influenced by statistical fluctuations. The number of detected photons n_{dph} as function of the incident number of photons N_{ph} can be approximated by the following expression:

$$n_{dph} = N_c \left(1 - e^{\left(-\frac{PDE \cdot N_{ph}}{N_m}\right)}\right) \tag{2.4}$$

Where N_m is the total number of micro cells in the SiPM and PDE is the Photon Detection Efficiency.

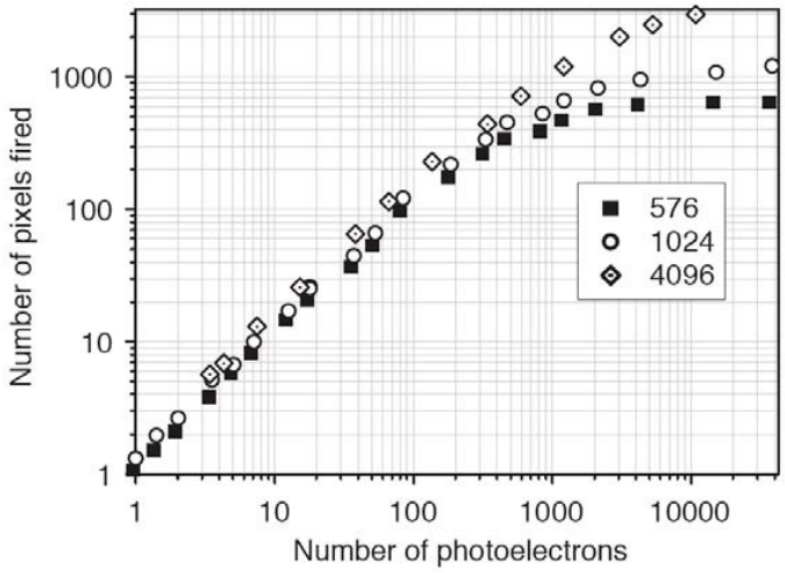

Figure 2.6: Response of SiPMs with different number of micro cells to laser light of increasing intensity. The SiPM with a greater number of cells has a larger response extension.[5]

The features analyzed in this work of thesis are:

1. Gain
2. Noise Measurement

2.3 Photodetectors for Cherenkov observations

Being the PMT a mature and well known technology, it has been used in most of the IACT experiments. SiPM, nevertheless are becoming a promising alternative.

In fact PMTs, even if they are characterized by a high gain (10^5-10^7) have the major problem of aging through the years. The aging depends both on how the quantity of light interacting with the device and on how much the device is strained. Being the night sky very bright (typically >100MHz on a Cherenkov camera pixel) they can not be used to their full gain because of the many photons they interact with, therefore PMTs are operated at lower gains in order to limit the aging factor. Also, because of the lower gain they need to be pre-amplified before the reading. SiPMs do not have this kind of problems: they don't age and can be used at higher gains. SiPMs also can tolerate accidental illumination, but when used with high currents (due to many photons arriving to the detector) the voltage drop on the quenching resistance self-restrains the sensor. Silicon in fact, is sensitive to all wavelengths up till the Silicon band gap, in the infrared region of the spectrum. This means that in order to operate with Si it is necessary to cover the detectors with a coating that only allows UV radiation to interact with the diode otherwise the high night sky luminosity in the visible band would lead to a large increase in the already high noise rate. Finally, while PMTs allow the creation of large sensors (i.e many inches in diameter), SiPM do not: a square inch of Silicon has a capacitance so high that the noise at the preamplifier output, which follows the linear equation $noise \sim a+b \cdot C$ (where a, b are constants and C is the capacitance), becomes enormous. In case a large sensor is necessary, an alternative approach must be investigated, such as, for example summing arrays of small sensors singularly amplified and to sum up the result.

Other features that make SiPMs interesting are:

- low temperature and bias voltages fluctuations (50 V $\sim$ 70 V);
- low power consumption ($< 50 \mu W/mm^2$);
- insensitive to magnetic fields up to 15 T;

- mechanical robustness;
- compact and rugged;
- no damage from accidental and prolonged illumination;
- cheap;
- no aging over the years.

At the moment for NUV (near ultraviolet) range the PDE is higher for last generation PMTs, but considering the improvement trend of SiPMs it is likely that they will soon surpass PMTs. To summarize, one can say that SiPMs have become widely accepted as promising photon detectors for IACT even though the current stage of development is still far from the theoretical optimum.

Chapter 3

Measurements and Data Analysis

This chapter describes the techniques used in order to perform the various measurements of the SiPM properties. The instrumentation used will not be described in this chapter but will be included in the Appendix A.

The characterization of a SiPM is divided in different stages: the basic property for the SiPM operation, the breakdown voltage, can be easily determined measuring current versus bias voltage. For the photodetection performance, a dark room is needed, and waveforms are collected with a digital oscilloscope and analyzed with the dedicated software.

3.1 $\mathbf{V}_b$ Measure

The first step, necessary to determine the operational voltage for all the remaining tests, is the measurement of the reverse current. This process allows to determine the diode breakdown voltage V_b. The measure is carried out by a scan of the reverse current as a function of the bias voltage. Two different regimes can be identified:

- For $\mathbf{V} < \mathbf{V}_b$ the current is mainly due to generation of photo electrons in the surface region around the diode, it is the non-avalanche mode of the *pn* junction and $I_{pre-BD} \sim V$ has a linear behavior.
- For $\mathbf{V} > \mathbf{V}_b$ the avalanche process has started and the current has a parabolic breakdown: the dark rate is proportional to the overvoltage $V_o = V - V_b$,and the gain G is again proportional to V_o, so $I_{post-BD} = q \cdot G \cdot N_{dark} \sim q \cdot V_o \cdot V_o$.

The breakdown voltage is a function of the temperature, therefore we monitored carefully the temperature.

3.2 Noise Measurements - Dark Rate

One limiting factor for both the performance and the size of the silicon photo multiplier is the dark rate.

Typical total dark count rates of current devices at room temperature are 150kHz over square millimeter. As the dark counts are dominated by thermal generation it can, in most cases, be adequately suppressed by a thin active volume and by moderate cooling.

3.2.1 Experimental set-up

The set up used for the dark characterization consists in a dark chamber, containing the SiPM and the preamplification stage and a digital oscilloscope to sample the output voltage signal (in our case DRS4, see *Appendix* A). The output of the preamplifier is sampled at a frequency of 2 GHz and waveforms containing 1024 voltage values are saved. In the case of a light signal, the trigger from the LED pulser can be used so that the SiPM signal is expected always in the same relative position in the data frame. In the case of dark measurements (no LED) the trigger is random. The waveform acquisition was repeated for different voltages at a given temperature of 26.9^{o}C. The device used in this measurements was a FBK SiPM of the size of 1x1 mm^2 and cells of 50x50 μm^2.

3.2.2 Data Analysis

The first step for the data analysis is a waveform conditioning, aimed to reduce the SiPM pulse duration. This is necessary for the long tail, that creates a pile-up probability that increases with the event rate, which can cause problems to both the pulse identification and its amplitude assignments. The filtering technique used is called DLED. The DLED waveform is obtained by subtracting to the original waveform a slightly delayed replica. This way, only the fast rising edge is preserved while the long tail is suppressed. The DLED signal can have a pronounced undershoot if the SiPM signal has a fast decay component, which needs to be eliminated. A pulse identification procedure is then launched and an array containing the time stamps of events having peak above a the threshold, which had been set at half the amplitude of the single cell response, is created. One value to set is the temporal

delay between the signal and the replica: by trial and error we set it to 10 samples (corresponding to 5 ns) to maximize the peak signal-to-noise radio. The peakfinder algorithm is than applied to the new waveform: peak height is now an arbitrary number, proportional to the peak height in mV before the DLED.

When all the events in a waveform are identified with a time stamp two arrays are created containing respectively the time distance between consecutive events and pulse amplitudes. The combination of the two arrays gives all the relevant informations regarding the noise properties of the device, in fact all the different noise components are visible (as shown in Fig.3.1):

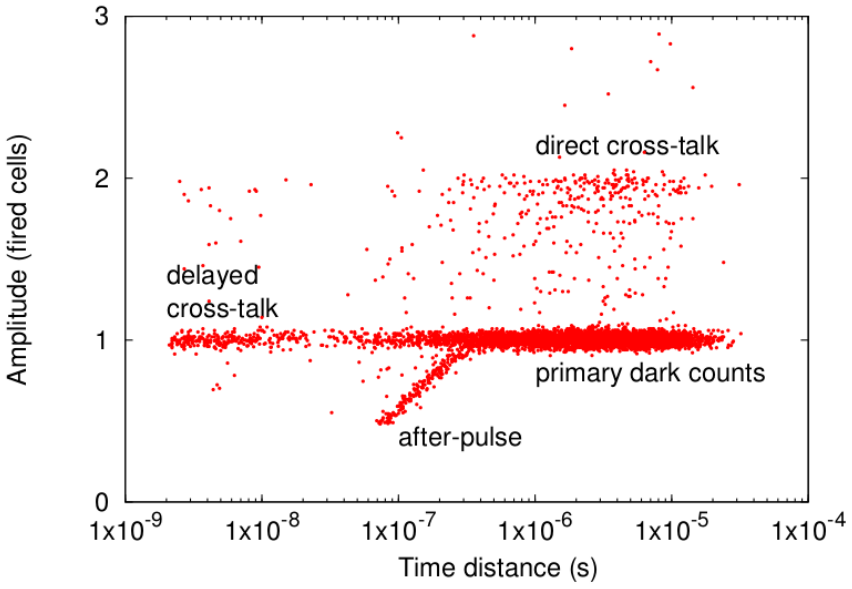

Figure 3.1: Scattering plot of the pulse amplitude as a function of distance from the previous event at a fixed voltage [3].

- **Primary dark counts:** this cloud follows the Poisson distribution as will be shown later.
- **After-pulses**: a cell that fired and is recharging, fires again giving an incomplete charge amount, immediately after a normal pulse.
- **Direct optical Cross Talk:** during a primary cell discharge a photon is emitted and absorbed in the depletion region of a neighboring cell triggering a second discharge in coincidence with the first one.

- **Delayed optical Cross Talk:** due to the fact that during the primary cell discharge, a photon is emitted and absorbed in the non-depleted region beneath a neighboring cell triggering a second discharge with a certain delay from the first one because of the diffusion time of photo-generated carriers.

In a histogram of the delay times of consecutive peaks, one expects to observe an exponential distribution (since the peak production is a Poisson process). The presence of effects mentioned above makes the analysis more complicated, and the Poisson rate cannot be naively obtained as "number of peaks divided by acquisition time" (uncorrected dark rate). Afterpulses must be removed by hand before building the histogram. Direct crosstalk is not an issue, since it only causes an increase in the peak height. Delayed crosstalk causes an excess of peaks with short time delays, which must be excluded when the Poisson rate is obtained from the exponential distribution ("corrected dark rate").

3.3 Measurements under illumination

In Fig. 3.2 several waveforms taken with LED illumination and LED trigger are shown (figure from literature). On the left side the baseline can be measured, the peak amplitude can be evaluated as the difference between the maximum of the V values (minimum is this case) and the baseline. On the right the histogram of peak amplitude is shown.

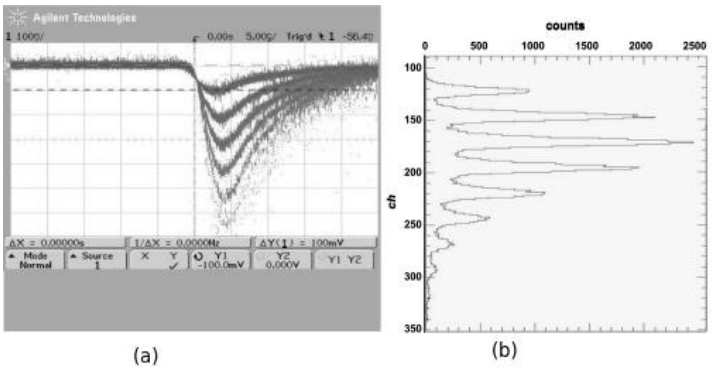

Figure 3.2: (a) Spectrum shown in the oscilloscope. (b) Spectrum of the low photon flox.

From the amplitude histogram one can obtain several parameters such as gain, crosstalk probability (PCT) and count rate.

3.3.1 Experimental setup

The experimental setup of the characterization under illumination consists in a chamber containing the SiPM, the amplification stage and a blue emitting LED as light source, coupled to a fast pulse generator and to a digital oscilloscope and providing trigger to the data acquisition system. The Led intensity can be adjusted with a numbered potentiometer (0-1000 arbitrary units). In all our measurements we used an LED with a wavelength of 380 nm. The acquisitions have been carried out at a temperature of T=27^{o}C.

The measure has been carried out in two different ways:

1. By setting the LED intensity to 760 and operating at different voltages.
2. By using a second SiPM as reference and operating at different voltages over V_b and at different intensities of the LED (I = 700, 740, 780, 810, 840).

3.3.2 Data analysis

For each value of overvoltage a spectrum similar to the one shown in Fig. 3.3 is obtained.

Peaks are searched for a given window, at the expected delay from the pulser trigger signal. The data analysis consists of a Gaussian fit of the spectrum obtained for each voltage and each intensity of the LED (see Fig. 3.4).

On the left, the histogram of peak amplitudes: the red curves are gaussian fit to the histogram peaks corresponding to 0,1,2.. detected photons. In the middle, a plot of the area of the gaussian, giving the number of events per peak amplitude, with statistical uncertainties. The fit curve is a Poisson distribution modified to include crosstalk probability, by mean of the following equation [2]:

$$f_k(p, L) = \frac{e^{-L} \cdot \sum_{i=0}^{k} B_{i,k}[L(1-p)]^i p^{k-i}}{k!} \tag{3.1}$$

Where: L is the parameter (mean value) of the Poisson distribution, p is the probability to have a secondary event produced by the first one,k is a parameter and $B_{i,k}$ is, for $i \neq 0$, $k \neq 0$:

$$B_{i,k} = \frac{k!(k-1)!}{i!(i-1)!(k-i)!} \tag{3.2}$$

Poisson rate and PCT are obtained by the fit. On the right: plot of the average peak height from the left plot. A linear fit gives the gain of the SiPM and of the amplifier, in mV/phe.

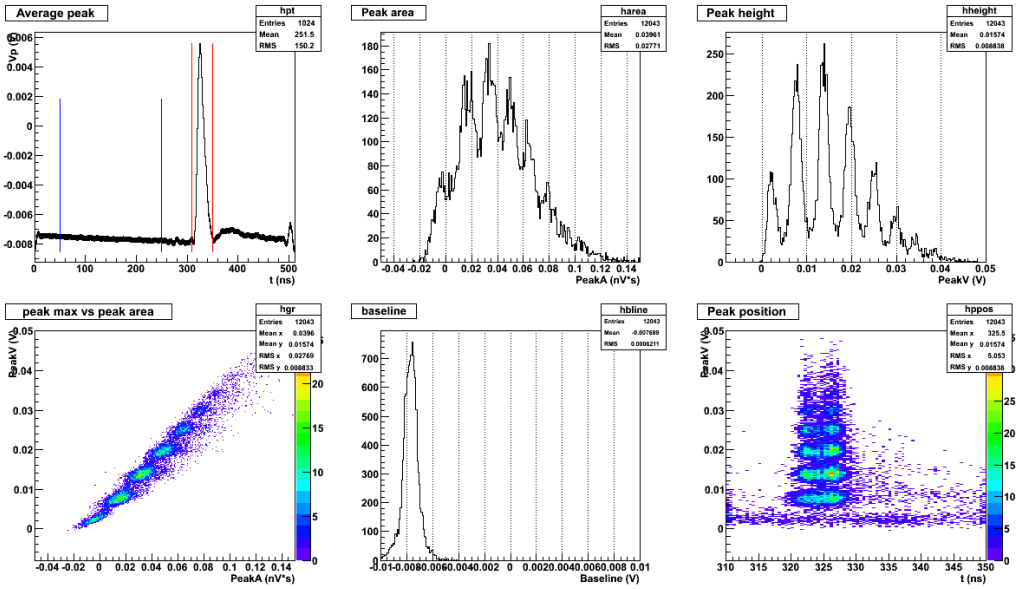

Figure 3.3: Top left: average of all data frames:the coloured lines indicate the regions where the baseline (blue) and peak amplitude (red) have been measured. Top center:peak area (not used). Top right: histogram of the peak amplitude. Bottom left:scatter plot of peak area and peak amplitude. Top center:histogram of baselines. Top right: peak amplitude versus position frame.

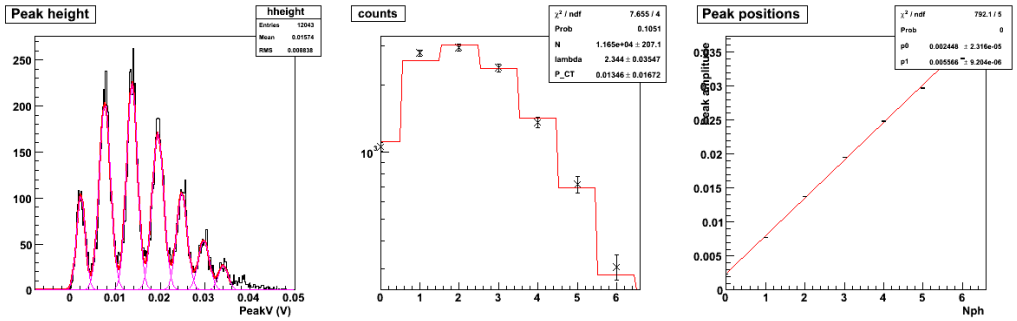

Figure 3.4: Gaussian fit of the spectrum at led intensity of 810 and voltage of 28.6 V.
[2]

Chapter 4

Experimental results and discussion

In this chapter we describe the results we obtained characterizing a novel NUV SiPM prototype by FBK.

4.1 V_B Measure

The experimental measured reverse current is shown in the Fig. 4.1.

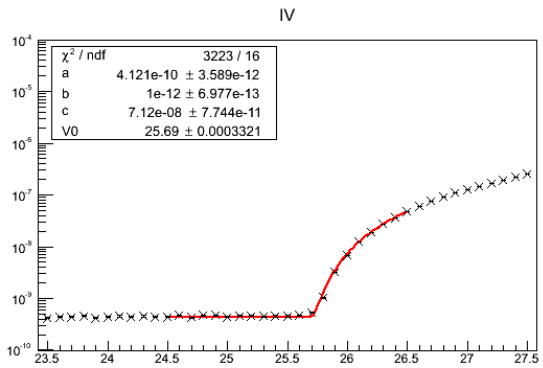

Figure 4.1: Measured reverse current at 25°C of a single pixel. Two different current regimes with respect to the applied voltage are identified.

The two different regimes described in the previous chapter are clearly shown: the current is linear in V for voltages inferior to V0 = 25.69 V and has a quadratic behavior for voltages higher than V0. The result has been calculated trough the functions:

$$I = a + b \cdot V for V < V0 \tag{4.1}$$

$$I = a + b \cdot V + c \cdot V^2 for V > V0 \tag{4.2}$$

From this measure the breakdown voltage is found to be $V_b = 25.69 \pm 0.10$ V. The error associated with this value is mainly due to the HP 41423 resolution which is about 10 mV. The statistical error and the error due to the temperature dependence are much smaller and can be neglected. Given such a low breakdown voltage, typical values of the bias voltage are around 30 V. This should be compared with $\sim$ 1000 V for a PMT.

4.2 Primary Dark Count Rate

The analysis of the DLED signal produced a scatter plot such as the one shown in Fig. 4.2

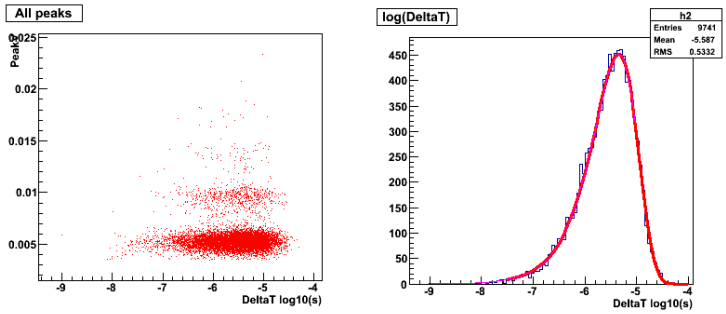

Figure 4.2: (a) Scatter plot of pulse amplitude (V) as function of $\log_{10}$ of the time distance at 2.5V of over-voltage. (b) Histogram of the time delay array, the solid red line is the Poisson fit of the data.

The analysis was meant to calculate the primary dark rate therefore events related to afterpulses and crosstalk have been removed from the data.

The uncorrected dark rate is simply given by the number of peaks over the total acquisition time: this is an overestimate of the intrinsic dark rate, since boot delayed crosstalk and afeterpulse affect it. An unbiased measurement can be done by fitting the Δt histogram after removing the afterpulse.

The result of the analysis is shown in Fig.4.4 Dark rate increases rapidly with overvoltage with values around several 100's kHz per mm^2, to be compared with a total $\sim$ 10 kHz for a multi-alkali PMT.

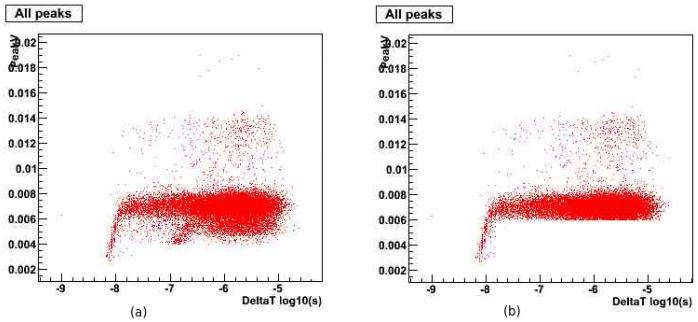

Figure 4.3: (a)Scatter plot of amplitude (V) as function of time distance, the afterpulses can be clearly seen in this image. (b) Filtered scatter plot of the amplitude as function of time distance.

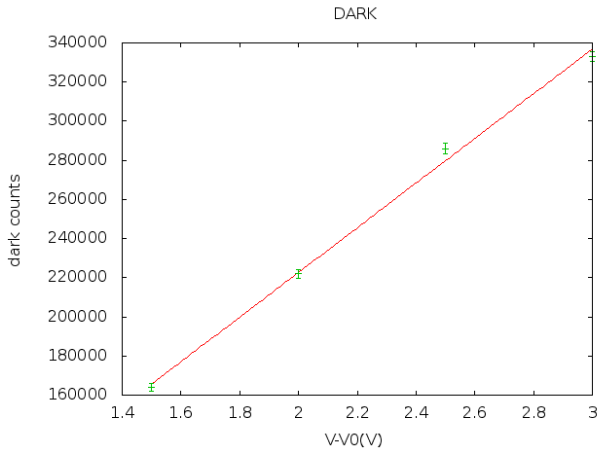

Figure 4.4: Dark rate of photomultiplier versus overvoltage at T=26.9^{o}C.

4.3 Measurements under illumination

The histogram of peak amplitudes can be fitted as sum of gaussians as shown in Fig. 3.4 and analyzed as described in the previous chapter. Excluding the fist peak (corresponding to the zero signal) a linear fit of peak amplitude versus number of detected photons gives the sensor gain (including the preaplificator gain). A modified Poisson fit of the number of frames having 0,1,2.. peaks gives the detected photon rate (or relative efficiency) and the crosstalk probability (see sect. 3.3.2).

4.3.1 Gain

We estimated the gain of the SiPM through the interpolation described in the previous chapter. Gain as a function of overvoltage is shown in the Fig. 4.5.

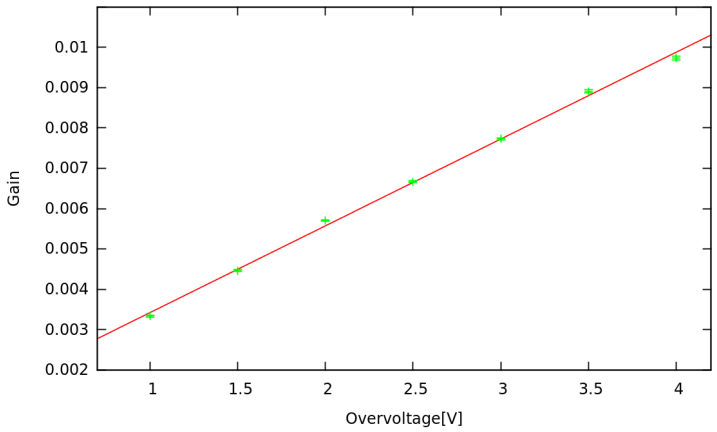

Figure 4.5: Gain versus $V - V_b$

It clearly shows a linear behavior. In principle, this implies we can define gain with precision by setting an adequate overvoltage. In reality, the dependence of the dark rate and crosstalk on overvoltage makes this determination of the operating point a complex procedure where advantages and disadvantages must be balances. The values of a few mV per photon are suitable for IACT applications, given the typical noise values of the DAQ electronics (< 1 mV).

4.3.2 Crosstalk probability

The measure with the light source allows also the calculus of the crosstalk probability. This is the most difficult measurement, it requires a significant statistics and it is affected by several systematics. The results of our measurements is shown in Fig. 4.6.

We expect an increasing trend independent from the LED intensity, with PCT values of a few percent to a few tens of percent. The uncertainties in Fig. 4.6 are the statistical errors from the modified Poisson fit. The measurements follow very well our expectations.

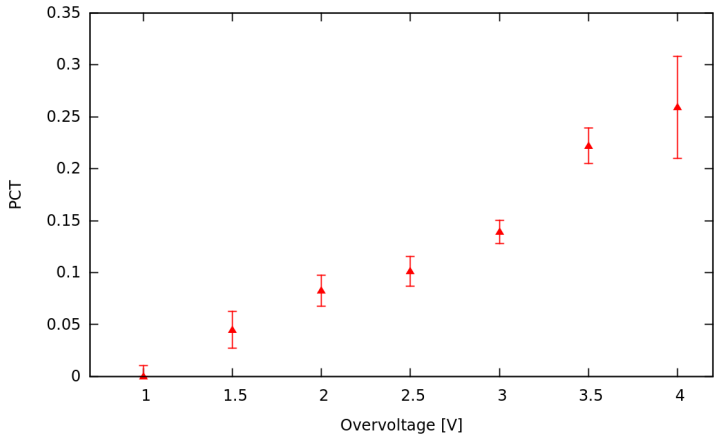

Figure 4.6: PCT versus $V - V_b$

4.4 Relative Efficiency

As shown in the previous sections, both gain and dark count rate grow linearly with the overvoltage. Another feature that can be calculated from the light measurements is the coefficient λ of the Poisson distribution. The following plots show the dependence of λ to the overvoltage for both the reference NUV07 (which had been set at a determined value of overvoltage $V_0 = 2.5V$) and the SiPM NUV18 for the different intensities of the LED:

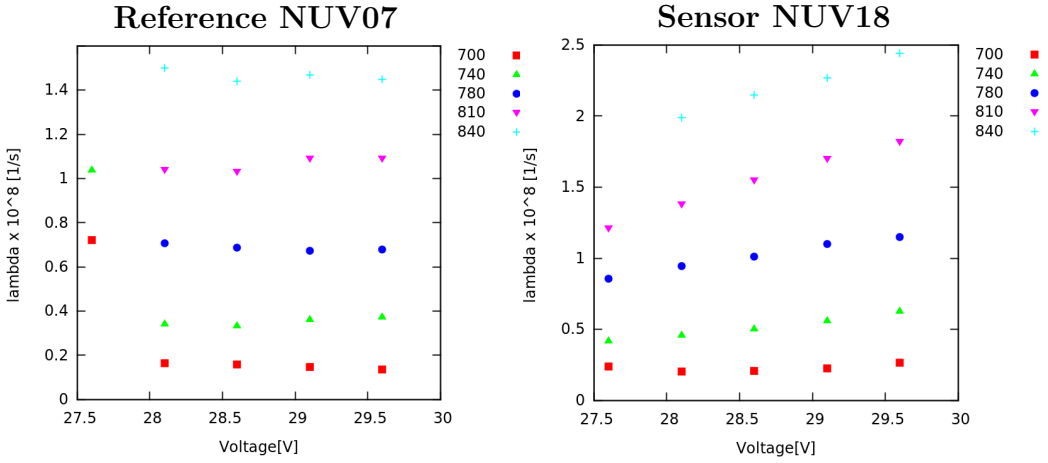

Reference Nuv07 Sensor NUV18

By putting together two sensors we obtain the graph of the efficiency shown in Fig. 4.7.

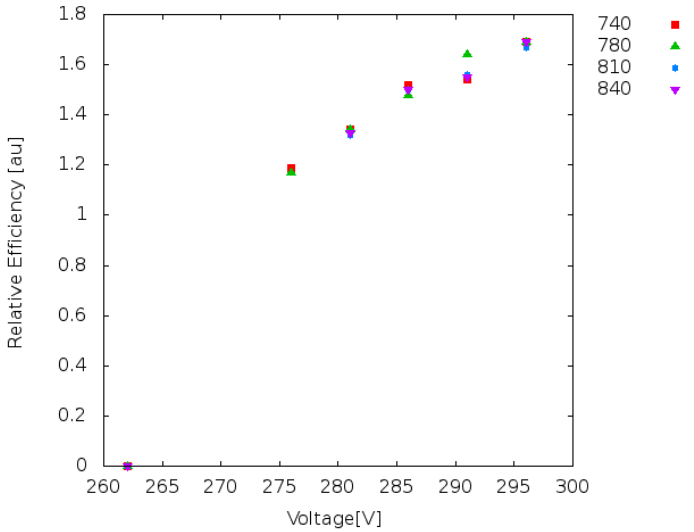

Figure 4.7: Relative efficiency versus voltage.

An useful plot is the scatter plot of dark rate versus efficiency (see Fig. 4.8). For increasing values of overvoltage, both dark rate and relative efficiency increase. While for lower overvoltage values the efficiency increases significantly, at higher voltages efficiency is saturating while dark rate increases rapidly.

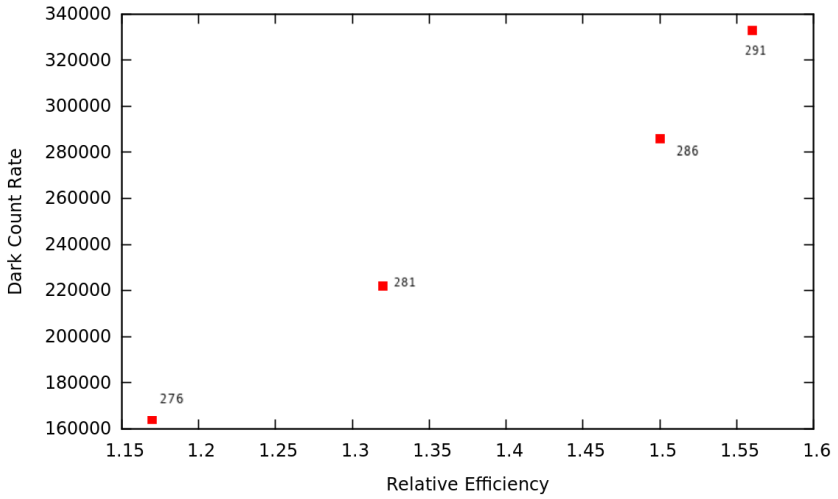

Figure 4.8: Relative efficiency versus Dark Count Rate. The labels on the points indicate the applied voltage, for example 276 indicates a voltage of 26.6 V

Chapter 5

Conclusions

In this work we studied the performance of SiPM sensors. Several detectors have been tested, and in particular this thesis has focused on the characterization of a FBK NUV SiPM.
The results found are coherent with the expected values.

For a complete characterization some additional measurements are required: some measurements need to be completed with an analysis of systematic effects; other figures of merit, for example the temperature dependency of various parameters, require an improvement of the instrumental setup in order to be evaluated.

Appendix A

Instrumentation

This work was performed in the MAGIC-CTA laboratories of the Department of Physics and Astronomy of the University of Padova. The most relevant instruments are the amplifier, the LED pulse generator, the digital oscilloscope and the high voltage source-picoamperometer unit.

The amplifier used is a fast preamplifier, with a gain of ∼30 mV/phe. It was developed and optimized for a fast discharge time,at the expense of some gain, with an internal passive high-pass filter. The LED-pulser used is the Picoquant PDL 800-B [10] (Picosecond Pulsed Diode Laser Driver) is shown in Fig. A.1 and provides driving pulses for the connected laser/LED heads with repetition rates up to 40 MHz.

Figure A.1: PDL - Picosecond Pulsed Diode Laser Driver.

The PLS is a sub-nanosecond pulsed LED (see Fig.A.2), in particular the one used for this analysis was a LED emitting in the range of the ultraviolet spectral range in order to reproduce the Cherenkov radiation ($\lambda = 380nm$). [12]

Figure A.2: PDL 800-B/-D/828 (PLS LEds).

The HP41423A is a high voltage source/monitor unit (HVU). It measures current when operating as voltage source and measures voltage when operating as current source. It has been used for the reverse current measurements. The features that characterize this instrument are:

- Voltage from ±10mV to ± 1000 V
- Current range: ± 50pA to ±10mA
- Measurment resolution of 2 mV 2pA
- Accuracy of .05%V and 1%I.

The DRS4 evaluation board, is the instrument used for sampling the voltage output of the SiPM circuits.
It is developed by Paul Scherrer Institute (PSI) as an evaluation platform for the DRS4 chip (Domino Ring Sampler). It has the following characteristics:

- Four 50Ω terminated input channels with SMA connectors.
- Active input buffers which result in an analog bandwidth of 700 MHz (-3dB).
- High bandwidth analog switches for internal voltage calibration.
- Precision clock for internal timing calibration, reaching a precision of a few pico seconds.
- One DRS4 chip, capable of sampling the four input signals simultaneously from 0.7 GSPS to 5 GSPS with 1024 sampling points each.
- One AD9245 ADC to digitize signals from the DRS4 chip.
- One Xilinx Spartan 3 FPGA for readout control.
- A 16-bit DAC to generate all on-board control voltages.

- A serial EEPROM containing serial number and calibration information.
- Internal trigger with user-defined thresholds on any of the four channes.
- Triggering on combinations of the four channels (AND/OR) for coincidence measurements.
- An external trigger input (TTL input 50Ω terminated) with a MCX connector.
- Trigger output for daisy-chaining of several evaluation boards.
- Clock input and output connectors (MCX) for synchronizing several evaluation boards.
- A USB 2.0 interface for data readout. This interface also powers this board. The maximum readout rate is about 500 events per second.
- Several headers for debugging of all important control signals with an oscilloscipe or logic analyzer.

Appendix B

An exercise: measure of c

Our setup can be easily adapted for a quick measure of the speed of light. In order to do this, the LED PLS has been used as light source, coupled with the pulse generator PDL 800-B and a fast digital oscilloscope.

We trigger on the prompt signal given by the pulse generator. The measure has been carried out by measuring with the cursors the time after the trigger at which the signal rises to 50 % of the maximum. By positioning the SiPM at different distances from the light source we obtain the results in the table:

Distance Δx (m)	time (ns)	$t_{err}(ns)$
0	9.05	0.45
0.1	9.45	0.60
0.2	10.30	0.65

The uncertainty is found as the half width of the peak curve thickness, given by the oscilloscope persistence.
The main limitation for this measurement is due to the fact that by operating inside the dark chamber the maximum distance is about 20 cm. Even under these conditions it is remarkable how we could calculate the speed of light, with some precision, as: $v = \Delta x/\Delta t$.
We find:

$$c = 3.02 \times 10^8 \pm 4.03 \times 10^7 m/s \tag{B.1}$$

with a relative uncertainty of about 10%.

Bibliography

[1] Valeri Saveliev *Silicon Photomultiplier - New Era of Photo Detection, Advances in Optical and Photonic Devices*, Kim Young Kim, ISBN:978-953-7619-76-3, InTech, 2010.

[2] S. Vinogradov, T. Vinogradova, V. Shubin, D.Shishikov, K. Sitarsky *Probability Distribution and Noise Factor of Solid State Photomultiplier Signals with Crosstalk and Afterpulsing*, Nuclear Science Symposium Conference Record (NSS/MIC), 2009 IEEE.

[3] Claudio Piemonte, Alessandro Ferri, Alberto Gola, Antonino Picciotto, Tiziana Pro, Nicola Serra, Alessandro Tarolli, Nicola Zorzi *Description of an automatic procedure for the characterization in dark of silicon photomultipliers*, Nuclear Science Symposium and Medical Imaging Conference (NSS/MIC), 2012 IEEE

[4] Gianmaria Collazuol, *Silicon Photo-multipliers*, Ferrara seminar, *http://collazug.home.cern.ch/collazug/*

[5] N. Otte, *The Silicon Photomultiplier - A new device for High Energy Physics, Astroparticle Physics, Industrial and Medical Applications*, SNIC Symposium, Stanford, California, 2006.

[6] Ignacio Dièguez Estremera, *Pulse Preamplifiers for CTA Camera Photodetectors*, 2011.

[7] Roberto Pagano, *Operative Parameters of Si Photomultipliers.*

[8] *https://srs.fbk.eu/optimization-sipm-technology*

[9] C. Piemonte , Battiston, Roberto, Boscardin, M.Dalla Betta, G.F.more authors *Characterization of the First Prototypes of Silicon Photomultiplier Fabricated at ITC-irst*, IEEE Trans. Nucl. Sci., 54,1, (2007) 236-244.

[10] *https://www.picoquant.com/products/category/picosecond-pulsed-driver/pdl-800-b-picosecond-pulsed-diode-laser-driver*

[11] *https://portal.cta-observatory.org/*

[12] *http://www.psi.ch/drs/evaluation-board*